

THE DIRECT IMPLICATIONS OF WARMING ON THE PHENOTYPE AND UNDERLYING FUNCTIONAL TRAITS OF MARINE PHYTOPLANKTON

KIRRALEE G BAKER

MAY 2016

A Thesis Submitted In Fulfillment Of The Requirements For The Degree Of Doctor Of
Philosophy In Science

Plant Functional Biology And Climate Change Cluster, School Of Life Sciences,
University Of Technology Sydney

CERTIFICATE OF AUTHORSHIP/ORIGINALITY

This thesis is the result of a research candidature conducted jointly with another University as part of a collaborative Doctoral degree. I certify that the work in this thesis has not previously been submitted for a degree nor has it been submitted as part of requirements for a degree except as part of the collaborative doctoral degree and/or fully acknowledged within the text.

I also certify that the thesis has been written by me. Any help that I have received in my research work and the preparation of the thesis itself has been acknowledged. In addition, I certify that all information sources and literature used are indicated in the thesis.

Kirralee G. Baker

This thesis is dedicated to my everlasting satellites RB and PB, who always guide me and initially inspired me to discover the natural world, and DR who since joining my path, has filled my life with overwhelming happiness, love and adventure.

ACKNOWLEDGEMENTS

In preparation of this thesis and the work it presents, I would like to thank my thesis committee members– Martina Doblin and Peter Ralph for your counsel. And thank you also to all the current and past members of the Aquatic Processes Group and the Coastal oceanography and algal research team. In particular, warmest thanks to Drs Katherina Petrou, Daniel Nielson, Louiza Norman, Christian Evenhuis, Milan Szabo and Joey Croswell for your patience but particularly your wisdom and expertise, and to Charlotte Robinson, Michaela Larsson, Lauren Messer and Dale Radford, for your many insightful and understanding discussions.

Thank you to Assoc. Prof. Justin Seymour, Drs Allison McInnes and Christian Evenhuis, and Dale Radford, Charlotte Robinson, Lauren Messer and Marco Alvarez Rodriguez who have provided support in the form of thoughtful discussions, data collection, analysis and methodologies that have allowed this thesis to come to fruition. Your individual contributions are acknowledged within this thesis.

Throughout this research I have been in receipt of financial support from a number of sources and would like to thank the Australian Government for their provision of an APA scholarship, and the School of Life Sciences and C3 Cluster for providing research funding.

TABLE OF CONTENTS

CERTIFICATE OF AUTHORSHIP/ORIGINALITY.....	ii
ACKNOWLEDGEMENTS.....	iv
TABLE OF CONTENTS.....	v
LIST OF FIGURES	ix
LIST OF TABLES	xvi
LIST OF SUPPLEMENTARY FIGURES	xviii
LIST OF SUPPLEMENTARY TABLES	xix
DECLARATION OF THE CONTRIBUTION TO EACH CHAPTER	xxii
CHAPTER 1: GENERAL INTRODUCTION	1
1.1 Phytoplankton	2
1.2 The ecological and biogeochemical roles of phytoplankton	4
1.3 The biogeographical distribution of phytoplankton functional groups	7
1.4 Functional traits, trade-offs and phenotypic plasticity	9
1.5 Predicting responses of phytoplankton to anthropogenic climate change.....	11
1.6 The implications of warming on phytoplankton.....	12
1.7 Research objectives and thesis outline	14
1.8 Literature cited.....	16
CHAPTER 2: THERMAL PERFORMANCE CURVES OF FUNCTIONAL TRAITS AID UNDERSTANDING OF THERMALLY-INDUCED CHANGES IN DIATOM-MEDIATED BIOGEOCHEMICAL FLUXES	25
2.1 Introduction	26
2.2 Methods and materials.....	28
2.2.1 Experimental setup	28
2.2.2 Phenotype fitness.....	28
2.2.3 Morphological traits	29
2.1.1.1 Cellular volume	29
2.1.1.2 Frustule silicification.....	29
2.2.4 Physiological traits	30
2.2.4.1 Photophysiology.....	30
2.2.4.2 Chlorophyll <i>a</i> content.....	31
2.2.4.3 Primary productivity (¹⁴ C uptake).....	32

2.2.4.4	Uptake of nitrogen, phosphate and silicate	32
2.2.5	Data analysis.....	33
2.3	Results	35
2.4	Discussion.....	46
2.4.1	Thermal performance curves reveal phenotypic plasticity	46
2.4.2	Temperature driven changes in fitness and other functional traits.....	47
2.4.3	Phenotype-dependent functional roles.....	49
2.4.4	Implications and future research directions.....	51
2.5	Acknowledgements	53
2.6	Literature cited.....	54
2.7	Supplementary Figures	59

CHAPTER 3: FUNCTIONAL TRAIT PLASTICITY ENABLES THERMAL TOLERANCE IN A NATURAL PHYTOPLANKTON COMMUNITY FROM SOUTH EAST AUSTRALIA.....		62
3.1	Introduction	63
3.2	Methods and Materials	66
3.2.1	Sample collection and experimental setup	66
3.2.2	Assessment of community functional traits.....	67
3.2.2.1	Primary Productivity	67
3.2.2.2	Photophysiology	67
3.2.3	Biogenic silicon production.....	68
3.2.4	Diatom-specific frustule silicification	68
3.2.5	Cell-specific functional traits of the pico- and nano-phytoplankton community	69
3.2.6	Data Analysis.....	70
3.3	Results	72
3.3.1	Physicochemical and biological characterisation of Port Hacking.....	72
3.3.2	Thermally induced changes in functional traits of community	73
3.3.3	Temperature effects on pico- and nano-phytoplankton composition	76
3.3.4	Temperature effects on universal functional traits measured in pico- and nano-phytoplankton.....	78
3.3.5	Temperature effects on diatom specific functional traits	81
3.4	Discussion.....	84
3.4.1	Thermal responses of community-level functional traits and implications on biogeochemical cycling of carbon and silicon.....	84
3.4.2	Temperature-specific phenotypes and divergence within and between phytoplankton functional groups.....	86

3.4.3	Implications and further directions.....	88
3.5	Acknowledgments	90
3.6	Literature cited.....	91
 CHAPTER 4: SPATIAL MAPPING OF DIATOM PHENOTYPES REVEALS FUNCTIONAL TRAIT DIVERSITY BETWEEN TWO DISTINCT AUSTRALIAN OCEANIC PROVINCES.....		
		96
4.1	Introduction	97
4.2	Methods and materials.....	99
4.2.1	Sample collection	99
4.2.2	Physicochemical characterisation of seawater.....	99
4.2.3	Biological characterisation of seawater	99
4.2.4	Experimental set-up.....	100
4.2.5	Tracking cell-specific silicification and community-level biogenic silicon production.....	101
4.2.5.1	Cell-specific silicification.....	101
4.2.5.2	Diatom-community biogenic silicon standing stocks and rates of biogenic silicon production.....	103
4.2.6	Data analysis.....	104
4.3	Results	107
4.3.1	Physicochemical characterisation of Arafura Timor Shelf and Coral Sea	107
4.3.2	Biological characterisation of Arafura Timor Shelf and Coral Sea.....	111
4.3.3	Nitrate addition assays.....	112
4.3.4	Biogenic silicon production differs between Arafura Timor Shelf and Coral Sea.....	114
4.3.5	Morphotype-specific differences in silicification between Arafura Timor Shelf and Coral Sea	115
4.3.6	Patterns in morphotype-specific silicification	119
4.4	Discussion.....	123
4.4.1	Northern Australia: a medley of biogenic silicon production and carbon export potential	123
4.4.2	The role of nitrate limitation in regulating biogenic silicon production.....	125
4.4.3	Functional trait diversity between Arafura Timor Shelf, Coral Sea and the biogeochemical implications.....	126
4.4.4	Implications and future studies.....	127
4.5	Acknowledgements	129
4.6	Literature cited.....	130
4.7	Supplementary Figures	135

CHAPTER 5: WARMING PROMOTES SPECIALISATION TO SUPRA-OPTIMAL TEMPERATURE IN A TROPICAL DINOFLAGELLATE	136
5.1 Introduction	137
5.2 Methods and Materials	140
5.2.1 Establishment of high-temperature adapted strain and culture conditions	140
5.2.2 Experimental set up and sampling:	140
5.2.2.1 Reciprocal transplant assay to estimate costs of acclimation and adaptation	140
5.2.2.2 Thermal performance curves to examine fitness trade-offs	141
5.2.3 Characterisation of phenotype: trait analysis	142
5.2.3.1 Growth and viability	142
5.2.3.2 Cell size	142
5.2.3.3 Fatty acid composition analysis	143
5.2.3.4 Chlorophyll <i>a</i> analysis	144
5.2.3.5 Photophysiology	144
5.2.3.6 Net flux of dissolved nutrients	145
5.2.4 Data analysis	146
5.3 Results	148
5.3.1 Costs, benefits and reversibility of high temperature adaptation	148
5.3.2 Trade-offs and evolution of the thermal performance curve following HT adaptation	151
5.4 Discussion	163
5.4.1 High-temperature phenotype comprised of fixed and dynamic traits	163
5.4.2 High-temperature phenotype remains indistinguishable from the control-temperature phenotype under intermediate temperatures	164
5.4.3 Costs and benefits associated with high-temperature phenotype	165
5.4.4 Implications and further research	167
5.5 Acknowledgements	168
5.6 Literature cited	169
5.7 Supplementary Tables	174
CHAPTER 6: GENERAL DISCUSSION	175
6.1 The role of functional trait diversity in regulating biogeochemical cycling	176
6.2 Environmental ‘filtering’ on functional traits	177
6.3 The effects of thermal acclimation and adaptation on marine biogeochemical cycling	180
6.4 The emergence of new phenotypes from extant species	182
6.5 Perspectives for further research	184
6.6 Literature cited	188

LIST OF FIGURES

- Figure 1.1** Typology of functional traits (FTs) redrawn from Litchman and Klausmeier (2008). Trade-offs between many FTs have significant implications for the functional ecology of marine systems, as many of these traits are involved in resource acquisition and have direct control over biogeochemical fluxes. Physiological traits such as nutrient uptake directly affect the elemental cycles of C, N, P and Si; whereas, morphological traits such as cell size and frustule silicification regulate these biogeochemical cycles by influencing cell aggregation, cell sinking rates and vulnerability to grazing.9
- Figure 2.1** Thermal performance curves (TPC) of fitness in the cosmopolitan model diatom *T. pseudonana* showing growth rate as a function of temperature ($n = 33$, RSME =0.1). Each symbol represents a distinct biological replicate. The solid line corresponds to maximum likelihood estimate (MLE) with broken lines corresponding to the 95 % confidence intervals (CI) of the bell-shape function (Equation 2.1) estimated by parametric bootstrapping.38
- Figure 2.2** Thermal performance curves (TPC) of morphological traits in the diatom *T. pseudonana* portraying (a) cell volume ($n = 33$, $p < 0.01$, $R^2 = 0.34$); and (b) frustule silicification ($n = 31$, $p < 0.01$, $R^2 = 0.41$), as a function of temperature. Each symbol represents a distinct biological replicate. The solid line corresponds to maximum likelihood estimate (MLE) with broken lines corresponding to the 95 % confidence intervals (CI) of a linear regression both estimated by parametric bootstrapping.39
- Figure 2.3** Thermal performance curves (TPC) of *T. pseudonana* photophysiological traits relating to light acquisition and harvesting showing (a) Functional cross-sectional area of PSII ($n = 32$, $p = 0.03$, $R^2 = 0.59$); (b) Effective quantum yield ($n = 33$, $p < 0.01$, $R^2 = 0.32$); (c) Electron transport rate ($n = 33$, $p = 0.23$, $R^2 = 0.01$); (d) Reoxidation time of Q_A ($n = 33$, $p < 0.01$, $R^2 = 0.59$); (e) Saturating irradiance ($n = 12$); and (f) Light harvesting efficiency ($n = 12$), as a function of temperature. Cells were harvested from cultures grown at $50 \mu\text{mol photons m}^{-2} \text{s}^{-1}$, with each symbol representing a distinct biological replicate. Solid line corresponds to maximum likelihood estimate (MLE) with broken lines corresponding to the 95 % confidence intervals (CI) of a linear regression, all estimated by parametric bootstrapping. (e - f) Data shown are parameters derived from rapid light curves with a single biological replicate, hence no maximum likelihood estimates or confidence intervals.41
- Figure 2.4** Thermal performance curves (TPC) of physiological traits in the diatom *T. pseudonana* describing (a) primary productivity ($n = 32$, RSME =0.5); (b) chlorophyll content ($n = 29$, RSME =0.4); and (c) chlorophyll normalised productivity ($n = 29$, $p < 0.01$, $R^2 = 0.44$), as a function of temperature. Each symbol represents a distinct biological replicate. Solid lines correspond to maximum

likelihood estimate (MLE) with broken lines corresponding to the 95 % confidence intervals (CI) of the (a, b) bell-shape function (Equation 2.1), and (c) linear regression, all estimated by parametric bootstrapping.42

Figure 2.5 Thermal performance curves (TPC) of physiological traits in the diatom *T. pseudonana* depicting uptake of dissolved nutrients (a) nitrate ($n = 33$, $p = 0.039$, $R^2 = 0.10$); (b) nitrite ($n = 33$, RSME = 13.7); (c) phosphate ($n = 33$, RSME = 5.2); and (d) silicate ($n = 33$, RSME = 54.4), as a function of temperature. Each symbol represents a distinct biological replicate. Solid lines corresponds to maximum likelihood estimate (MLE) with broken lines corresponding to the 95 % confidence intervals (CI) of (a) linear regression, and (b - d) the bell-shape function (Equation 2.1), all estimated by parametric bootstrapping.44

Figure 2.6 A comparison of the thermal optimum (temperature range over which the maximum trait value is obtained), and niche width (temperature range over which trait value is positive) of various functional traits measured in the diatom *T. pseudonana*, which were parameterised by fitting the bell-shaped function (Equation 2.1). Symbols represent maximum likelihood estimate (MLE) and error bars correspond to the 95 % confidence intervals (CI), both estimated by parametric bootstrapping. Functional traits (FT) are sub-categorised into three groups (Group I, II and II) separated by the upper 95% CI for the thermal optimum and niche width for growth (broken grey lines).45

Figure 2.7 Thermal performance curves (TPC) of fitness (*grey band*) and other functional traits (FT) including primary productivity (*green band*), cell volume (*blue band*) and frustule silicification (*red band*) in the marine diatom *T. pseudonana* (CCMP 1335) originally isolated from the North Atlantic Ocean. Each confidence band represents the maximum likelihood estimate (MLE) with 95 % confidence intervals (CI), both estimated by parametric bootstrapping for each functional trait. Solid vertical lines correspond to the thermal window currently encountered in the North Atlantic Ocean (NAO) ranging from the minimum boreal winter temperature ($\sim 10^\circ\text{C}$) and maximum boreal summer temperature ($\sim 25^\circ\text{C}$), both estimated from monthly sea surface temperatures for December 2014 and July 2015 obtained from NOAA. Broken line depicts predicted estimates of future mean sea surface temperature (SST) warming of the NAO (Boyd et al. 2015).51

Figure 3.1 Sampling location of source water collected from Port Hacking National Reference Station (PH100) at 151.2190 E, 34.1160 S: approximately 3 nautical miles off the coast of Sydney, NSW, Australia. (Figure credit: V. van Dongen-Vogels)71

Figure 3.2 Gross primary productivity of surface (5 m depth) phytoplankton community at Port Hacking, NSW (PH100) sampled in October 2015 as a function of temperature. Symbols represent mean and error bars are the standard error of the mean. Letters above symbols indicate statistically significant difference between

treatments identified by Tukeys's honest significant difference (HSD) test $p < 0.05$.
 74

Figure 3.3 Community composition of the initial *in situ* Port Hacking (PH100) phytoplankton in the $<20\ \mu\text{m}$ fraction as determined by flow cytometry using cell-specific phycoerythrin fluorescence and forward scatter (FSC) properties: *Synechococcus* spp. (white bars), *Prochlorococcus* spp. (grey bars) and eukaryotes (black bars), as well as the community composition after 24 h at different assay temperatures. Note log scale on y-axis. 77

Figure 3.4 Growth rate (d^{-1}) and change in relative cell size (estimated from forward angle light scattering; FSC) from T_0 (%) of the (a) small ($<20\ \mu\text{m}$) eukaryotes, (b) *Prochlorococcus* spp., and (c) *Synechococcus* spp surface (5 m depth) populations at Port Hacking (PH100) after 24 h of exposure to a range of temperatures. Growth rate was calculated as the difference in cell abundance (using counts obtained by flow cytometry) between initial (T_0) and final (T_{24}) for each plankton group. Changes in cell size measurements were calculated as the difference of average bead-normalised FSC between initial (T_0) and final (T_{24}) for each plankton group, obtained via flow cytometry. Each symbol represents an individual replicate with the colour of the symbols reflecting the temperature treatment: 15 °C (cold; dark blue), 19 °C (control; light blue), 24 and 26 °C (intermediate; yellow), and 30 and 32 °C (hot; red). Where symbols are absent, positive growth was not observed.... 80

Figure 3.5 Biogenic (BSi) production of small diatoms ($<20\ \mu\text{m}$) from the surface Port Hacking pico- and nano-phytoplankton communities collected in October 2015. BSi production was estimated by multiplying cell-specific bead-normalised PDMPO fluorescence (i.e., the relative amount of silicon deposited) by abundance of PDMPO positive cells (i.e., the number of actively depositing cells). Growth was assumed to be equivalent to division rates of eukaryotes in the $<20\ \mu\text{m}$ fraction and was calculated as the difference in cell abundance (using counts obtained by flow cytometry) between initial (T_0) and final (T_{24}). Each symbol represents an individual replicate with the colour of the symbols reflecting the temperature treatment: 15 °C (cold; dark blue), 19 °C (control; light blue), 24 and 26 °C (intermediate; yellow), and 30 and 32 °C (hot; red). Broken line represents the maximum likelihood estimate of linear regression ($R^2 = 0.69$, $p < 0.001$). 81

Figure 3.6 Abundance of and cell-specific silicon (Si) deposition by diatoms from the pico- and nano-phytoplankton ($<20\ \mu\text{m}$) fraction of seawater samples sampled from Port Hacking (PH100). Both parameters were obtained using flow cytometry whereby diatoms were first distinguished as PDMPO positive cells and then counted. Si deposition was calculated as cell-specific bead-normalised PDMPO fluorescence. Symbols represent the mean of triplicate samples and the error is the standard error of the mean..... 82

- Figure 4.1** Stations (closed circles; numbered 1-10) sampled during a 5000 km transect from Broome to Brisbane aboard the RV *Southern Surveyor* during the Austral winter (July-August; SS2013_t03), including locations referred to in text. 106
- Figure 4.2** Physicochemical characteristics of surface water sampled within the Arafura and Timor shelf regions (ATS) and Coral Sea (CS) oceanographic regions (RV *Southern Surveyor*; July-August; SS2013_t03); (a) temperature, (b) salinity, (c) ammonium, (d) nitrate, (e) phosphate, and (f) silicate. 110
- Figure 4.3** Distribution of phytoplankton in three size classes from sampled from (a) surface, and (b) subsurface chlorophyll maximum (Cmax) from the Arafura-Timor Shelf (ATS) and Coral Sea (CS) estimated from pigments algorithms as in Vidussi et al. (2001), Hooker et al. (2005) and Uitz et al. (2008); picophytoplankton <2 μm (grey bars), nanophytoplankton >2 μm and <20 μm (white bars), and microphytoplankton >20 μm (black bars). Station numbers reflect those in Figure 4.1 and the dashed line represents the transition from the ATS to the CS. 111
- Figure 4.4** Boxplots of the (a) C:N, (b) Si:N, and (c) Si:C molar ratios of particulate organic matter sampled from stations sampled from the Arafura-Timor Shelf (ATS; open boxes) and Coral Sea (CS; grey boxes). The length of the box corresponds to the distance between the 5th and 95th percentiles. The solid line and dashed line inside the box represent the mean and median, respectively. The whiskers extend to the minimum and maximum values of the cluster and “n” is the number of values in each cluster. The grey dashed lines represent the typical values of C:N (6.6) reported by Redfield et al. (1963) and typical values of Si:N (1.1) and Si:C (0.13) for nutrient replete diatoms reported by Brzezinski (1985). Asterisks indicate statistically significant differences ($p < 0.05$) of the mean between clusters using Student’s t test. 113
- Figure 4.5** (a) Biogenic silica production (BSi; $\mu\text{mol Si L}^{-1} \text{d}^{-1}$) by diatoms at stations sampled within the Arafura and Timor shelf regions (ATS) and Coral Sea (CS), where closed symbols represent unamended seawater control and open symbols represent seawater supplemented with additional nitrate (NO_3^- ; 10 $\mu\text{mol L}^{-1}$) for samples collected from surface waters (5 m) and, when discernable, the subsurface chlorophyll maximum (Cmax; determined by the down-cast Chl *a* fluorescence profile). The error term is the standard error. Station numbers reflect those in Figure 4.1 and the dashed line represents the transition from the ATS to the CS. (b) BSi production ($\mu\text{mol Si L}^{-1} \text{d}^{-1}$) by diatoms at stations sampled within the ATS and CS. The length of the box corresponds to the distance between the 5th and 95th percentiles. The solid line and dashed line inside the box represent the mean and median, respectively. The whiskers extend to the minimum and maximum values of the cluster and “n” is the number of values in each cluster. Asterisks indicate statistically significant differences ($p < 0.05$) between clusters using Student’s t test. 114

- Figure 4.6** Relative fluorescence as a function of diatom abundance (<20 µm sized cells) for positively PDMPO-stained cells quantified by flow cytometry sampled from the Arafura-Timor Shelf (ATS; closed symbols) and Coral Sea (CS; open symbols). Relative fluorescence units (RFUs) were normalised to relative cell size (forward scatter; FSC) in order to determine relative differences in frustule silicification. Note the y-axis is log scale..... 115
- Figure 4.7** Illustrative images of new silicon (BSi) deposition by diatoms incubated with PDMPO for 24 h from stations sampled from the ATS (left) and CS (right) mounted on glass slides and observed under fluorescence microscopy. A DAPI long pass filter was used to visualise PDMPO-stained cells over the entire emission spectrum. Exposure time remained constant for all photos so that pixel intensity is indicative of relative differences in the amount of newly incorporated PDMPO. The scale bar (10 microns) and image brightness is the same for all images to emphasise differences in size and degree of frustule silicification between ocean region and taxa. 117
- Figure 4.8** Boxplot of integrated fluorescence of individual cells incubated with PDMPO for 24 h from stations sampled from the Arafura Timor Shelf (ATS; open boxes) and Coral Sea (CS; grey boxes) and quantified with fluorescent microscopy. Note that y-axis is a log scale. The length of the box corresponds to the distance between the 5th and 95th percentiles. The solid line and dashed line inside the box represent the mean and median, respectively. The whiskers extend to the minimum and maximum values of the cluster and “n” is the number of values in each cluster. Asterisks indicate statistically significant differences ($p < 0.05$) between clusters using Student’s t test. 119
- Figure 4.9** The average contribution of each morphological type towards biogenic silica (BSi) production by diatoms sampled from the Arafura Timor Shelf (ATS) and the Coral Sea (CS). The stacked bar graph represents output from similarity percentages (SIMPER) analysis which identified six morphological types that explained >98% of community BSi production (derived from multiplying cell abundance by the average integrated PDMPO fluorescence per cell). The remaining morphological types (e.g. *Pseudo-nitzschia*) contributed <2% and were grouped into ‘Other’ morphological types. The error terms are standard deviation. 120
- Figure 4.10** Relationship between physicochemical characteristics and new biogenic silica (BSi) production of the diatom community from samples incubated in the presence of PDMPO for 24 h from each oceanic region (Arafura-Timor Shelf and Coral Sea). The plot represents a distance-based redundancy analysis (dbRDA) ordination of new BSi production generated from a Bray-Curtis distance matrix and ocean physicochemical characteristics chosen by the significances of distance linear-based model (DisTLM) marginal tests. 122

Figure 5.1 Physiological characterisation of the tropical dinoflagellate *Amphidinium massartii* following three years (~500 generations) of exposure to control (CT) or +5 °C (HT) conditions (25 °C versus 30 °C). Mean trait values (\pm standard error of the mean, $n = 3$) of control-temperature (CT)-population and high-temperature (HT)-populations (open versus hatched bars, respectively) when assayed at control (25 °C) and high (30 °C) temperatures (blue versus red bars, respectively) of (a) growth, (b) cell volume, (c) unsaturation index (unsaturated:saturated fatty acids), (d) chlorophyll *a* content per cell volume, (e) maximum electron transport rate, and (f) saturating irradiance. Letters above bars represent Tukey's honestly significant difference (HSD) between groups ($p < 0.05$). 150

Figure 5.2 Thermal performance curves (TPC) of fitness in the dinoflagellate *A. massartii* depicting growth rate as a function of temperature in the control-temperature (CT)-population (blue symbols; $n = 36$, MSE = 0.0022) and high-temperature (HT)-population (red symbols; $n = 36$, MSE = 0.0017). Each symbol represents a distinct biological replicate. Solid lines represent maximum likelihood estimates (MLE) and broken lines correspond to the 95% confidence intervals (CI) of the bell-shaped function (Equation 5.4), of the CT and HT-populations (blue and red lines, respectively). 151

Figure 5.3 Exposure-response curves in the dinoflagellate *A. massartii* representing the percentage of viable cells (negative for SYTOX green nucleic acid stain) as a function of time (hours) of control-temperature (CT)-population (blue symbols; $n = 12$) and high-temperature (HT)-populations (red symbols; $n = 12$) assayed at the two highest temperatures (a) 40 °C and (b) 38 °C where growth was not observed. Each symbol represents a distinct biological replicate. Solid lines represent maximum likelihood estimates (MLE) of the exposure-response function of the CT- and HT-populations (blue and red lines, respectively). 153

Figure 5.4 Thermal performance curves (TPC) of photophysiological parameters in the dinoflagellate *A. massartii* portraying (a) effective quantum yield (Φ_{PSII}), and (b) non-photochemical quenching (NPQ) in the control-temperature (CT)-population (blue symbols; $n = 36$, MSE = 0.0012) and high-temperature (HT)-population (red symbols; $n = 36$, MSE = 0.0010). Each symbols represents a distinct biological replicate. Solid lines represent maximum likelihood estimates (MLE) and broken lines correspond to the 95% confidence intervals (CI) of the bell-shaped function (Equation 5.4), of the CT and HT-populations (blue and red lines, respectively). 158

Figure 5.5 Thermal performance curves (TPC) of gross primary productivity (GPP) in the dinoflagellate *A. massartii* as a function of temperature in the control-temperature (CT)-population (blue symbols; $n = 36$, MSE = 0.1235) and high-temperature (HT)-population (red symbols; $n = 36$, MSE = 0.1296). Each symbols represents a distinct biological replicate. Solid lines represent maximum likelihood estimates (MLE) and broken lines correspond to the 95% confidence intervals (CI)

of the bell-shaped function (**Equation 5.4**), of the CT and HT-populations (blue and red lines, respectively).....160

Figure 5.6 Thermal performance curves (TPC) of nutrient uptake (net flux of dissolved nutrients) in the dinoflagellate *A. massartii* depicting (a) NO_x (nitrate and nitrite), and (b) phosphate uptake in the control-temperature (CT)-population (blue symbols; n = 36, MSE = NO_x; 2.1618, PO₄;-0.0053) and high-temperature (HT)-population (red symbols; n = 36, MSE = NO_x; 1.9561, PO₄;0.0046). Each symbol represents a distinct biological replicate. Solid lines represent maximum likelihood estimates (MLE) and broken lines correspond to the 95% confidence intervals (CI) of the bell-shaped function (**Equation 5.4**), of the CT and HT-populations (blue and red lines, respectively).....161

Figure 6.1 Natural selection on functional trait (FT) expression via species sorting; a proposed hypothesis arising from data presented in this thesis (a) A combination of flow cytometry and fluorescent stain, PDMPO (ex. 355; em. 488) is used to target a diatom community (black symbols) within a natural picophytoplankton community. Mean PDMPO fluorescence of the diatom community as a measure of the degree of frustule silicification. (b) A thermal performance curve is constructed using cell abundance of diatom community (black line) consisting of multiple species (different colours) differing in their thermal characteristics e.g. thermal optima. For each temperature, a different species will be more numerically dominant. (c) Population statistics of the FT (e.g. frustule silicification) are reported for the diatom community (black line). The FT value (e.g. median PDMPO fluorescence) observed at each temperature is weighted by species abundance and therefore reflects the FT trait value of the most dominant species due to their numerical dominance. As a result, the median FT value of the community remains consistent across a large temperature range due to the shuffling of species that occurs at each temperature and therefore reflects the locally ‘optimal’ trait value.179

Figure 6.2 Hypothetical allocation tradeoff arising from findings presented in this thesis. An allocation tradeoff arises along a temperature gradient, between silicic acid distributed towards girdle band or valve synthesis. For each cell, the extreme upper and lower parts are valves, and the series of dashes on the sides represent girdle bands. At cold temperatures (cold colours), silicic acid is distributed towards valve synthesis resulting in small cells with thicker valves. At warm temperatures (warm colours), silicic acid is distributed towards girdle band synthesis resulting in larger cells with thinner valves.181

LIST OF TABLES

Table 1.1 Key phytoplankton functional groups (PFG) and their role in various marine biogeochemical cycles. Note that some illustrative species appear more than once and exemplifies that clustering of PFGs are based on similarities in ecological and/or biogeochemical role, rather than phylogeny.	6
Table 2.1 Estimated thermal performance curve (TPC) parameters and associated uncertainty calculated from parametric bootstrapping for each functional trait (FT) fitted using Equation 2.1 ; thermal optimum T_{opt} , trait value at thermal optimum and thermal niche width.	36
Table 2.2 Estimated thermal performance curve (TPC) parameters for functional traits (FT) fitted using linear regression and associated uncertainty calculated by parametric bootstrapping, including: the proportional change in trait value per degree Celsius relative to the thermal optimum (T_{opt}) for growth (Δ °C) and trait value at thermal optimum.	37
Table 3.1 Physicochemical and biological characteristics of seawater collected from surface waters (5 m) of PH100. Where applicable, rates were obtained during daily incubation at <i>in situ</i> temperature and light characteristics. Where available, error is the standard deviation from $n=3$ replicates.	72
Table 3.2 Photosynthetic parameters of the phytoplankton community sampled from surface waters (5 m depth) of Port Hacking, NSW (PH100) and incubated at various temperatures for 24 h at 200 $\mu\text{mol photons m}^{-2} \text{ s}^{-1}$. Shown are F_V/F_M (maximum quantum yield; dimensionless), Φ_{PSII} (photochemical efficiency; dimensionless), ETR_{PSII} (electron transport rate through photosystem II; $\mu\text{mol } \bar{e} \text{ h}^{-1}$), NPQ (non-photochemical quenching; dimensionless), and τ (reoxidation time of Q_A ; μs). Those in bold indicates that there is significant difference ($p < 0.05$) between the assay temperature and ambient control (19 °C). Values given are the means, and values in parentheses are the standard error of the mean of measurements made on triplicate samples.	75
Table 4.1 Average inorganic silicate (SiO_4^{4-}), nitrate (NO_3^-), and phosphate (PO_4^{3-}) concentrations including elemental ratios for each station sampled in the Arafura-Timor Shelf and Coral Sea. At all stations, seawater samples were taken from surface waters (5 m) and, when discernable the sub-surface chlorophyll maximum (Cmax) as indicated by asterisks. The error term is the standard deviation. Hyphens indicate nutrient concentrations below instrumental detection limit ($< 0.02 \mu\text{mol L}^{-1}$).	108
Table 4.2 Average particulate organic carbon (POC), particulate organic nitrogen (PON), and biogenic silica (BSi) of each station sampled in the Arafura-Timor Shelf and Coral Sea. At all stations, seawater samples were taken from surface	

waters (5 m) and, when discernable the sub-surface chlorophyll maximum (Cmax) as indicated by asterisks. Error term is the standard deviation where applicable. 109

Table 4.3 Mean cellular dimensions and relative abundance (%) of diatom morphological types from the Arafura-Timor shelf and Coral Sea regions..... 116

Table 5.1 A summary of the statistically significant directional changes in thermal characteristics of traits measured in *A. massartii* following long-term high-temperature exposure (~500 generations at 30 °C)..... 152

Table 5.2a Estimated thermal performance curve (TPC) parameters and associated uncertainty for control-temperature (CT)- and high-temperature (HT)-populations calculated from parametric bootstrapping for growth rate and gross primary productivity fitted using Equation 5.4; thermal optimum T_{opt} , trait value at thermal optimum V_{max} , critical maximum temperature CT_{max} , critical minimum temperature CT_{min} and thermal niche width. The mean squared error (MSE) approximation provides a measure of uncertainty of the fitted function, whereas the 95 % confidence intervals (CI) provide a measure of uncertainty on the derived parameters. The shift in TPC associated with HT adaptation (ΔHT) was calculated as the difference in derived parameters between the CT and HT population. These differences were considered to be significant at $\alpha = 0.05$, if the 95% CI did not contain 0 (i.e. the null hypothesis rejected) and are indicated as bold text..... 154

Table 5.3 Estimated maximum carbon to nitrogen (C:N) and carbon to phosphorus (C:P) molar ratios in organic matter and associated uncertainty for CT and HT populations calculated using maximum trait value at thermal optimum (V_{max}) estimates from parametric bootstrapping for carbon (GPP), nitrogen (NO_x) and phosphorus (PO_4^{3-}) uptake. A change in molar ratios associated with HT adaptation (ΔHT) was calculated as the difference in derived parameters between the CT and HT population. These differences were considered to be significant at $\alpha = 0.05$, if the 95% CI did not contain 0 (i.e. the null hypothesis rejected) and are indicated as bold text. 162

LIST OF SUPPLEMENTARY FIGURES

- Supplementary Figure 2.1** Experimental setup of thermal gradient block. A temperature gradient was established across the aluminium block by circulating hot and cold water through milled channels at opposite ends of the block.....59
- Supplementary Figure 2.2** Gating logic for flow cytometric analysis of SYTOX incorporation in the diatom *T. pseudonana*. Cells were discriminated based upon chlorophyll fluorescence (692/40 nm) and forward scatter (FSC) (A). Gates were set on these populations to account for any auto fluorescence in these channels using cells not incubated in the presence of the stain (B). Gates were then set on populations with cells incubated in the presence of the stain (C). Heat-killed cells incubated in the presence of the stain were used as a positive control (D).....60
- Supplementary Figure 2.3** Gating logic for flow cytometric analysis of PDMPO incorporation in the diatom *T. pseudonana*. Standard fluorescent yellow-green beads (1 µm) were discriminated on fluorescence (530/40 nm) and forward scatter (FSC) (A). Cells were discriminated based upon chlorophyll fluorescence (692/40 nm) and forward scatter (FSC) (B). Gates were set on these populations to account for any auto fluorescence in the detection channel (469/29) with cells not incubated in the presence of PDMPO stain (C). Cells stained in the presence of PDMPO for 24 h (C).61
- Supplementary Figure 4.1** Vertical down-cast profiles of chlorophyll *a* (solid lines) measured in relative fluorescent units (RFU) from sites sampled within the Arafura Timor Shelf (1-6) and Coral Sea (7-10). Where present, dotted lines indicate sites where a subsurface chlorophyll maximum was discernable and with their location corresponding to the depth water samples were taken. Numbers on plot indicate bottom depth (m) for each station.135

LIST OF SUPPLEMENTARY TABLES

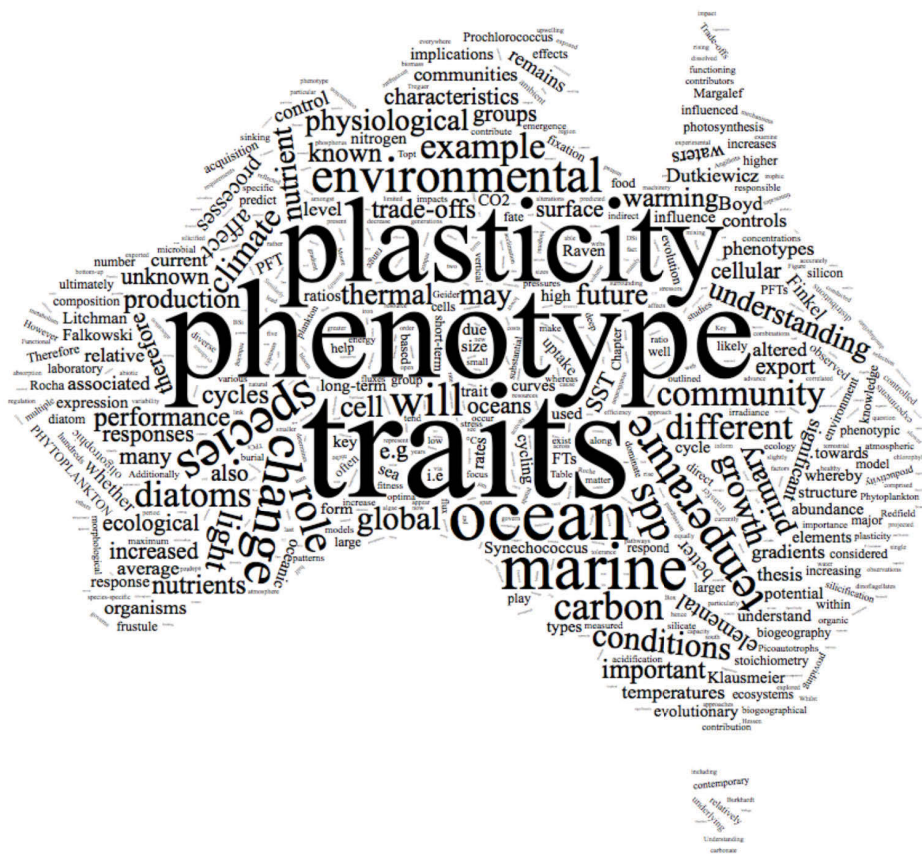
Supplementary Table 5.1 Net flux of nitrate (NO_3^-) and phosphate (PO_4^{3-}) in CT- and HT-populations of <i>A. massartii</i> at 25 and 30 °C estimated using cell size data from reciprocal transplant assay and nutrient data from thermal performance curve (TPC) experiments.	174
---	-----

SUMMARY

Marine phytoplankton mediate oceanic biogeochemical cycling by linking cellular metabolism with many elemental fluxes including C, N, P and Si. These elemental transformations are physiologically regulated processes that are influenced by phytoplankton phenotypes that change over different spatial and temporal scales. It is expected ocean warming (increasing sea surface temperatures; SST) will alter these patterns because temperature is the primary environmental control governing metabolism and growth in many phytoplankton groups. Whilst research on the effects of warming SST on biogeographical range shifts is advancing, it remains unknown how phytoplankton mediated biogeochemical transformations may be altered.

Focusing on patterns in species functional traits (FTs), this thesis applied trait-based approaches in laboratory and field studies to explore how biogeochemically-related FTs vary over environmental gradients. I quantified the thermal performance curves (TPCs) of FTs in representative species from two laboratory-cultured phytoplankton functional types to understand trade-offs associated with thermal acclimation and adaptation. To assess whether these laboratory-based patterns of FT trade-offs and expression were consistent in the field; I replicated a similar TPC experiment with a natural phytoplankton community. Finally, to understand how multiple environmental gradients interact to influence phytoplankton FT expression, I tracked a diatom-specific FT over northern Australia to spatially map the diatom phenotypes present to deduce the likely biogeochemical roles of the species in the region.

This thesis demonstrates the importance of understanding the relationship between the duration of thermal exposure, FT expression and trade-offs in regulating the phytoplankton phenotype, as all of these factors differentially affect species' growth rates (and therefore fitness and biogeography) but also the acquisition of C, N, P and Si, and therefore the marine cycling of these elements. Furthermore, ocean mapping of FTs proves insightful for understanding variability of biogeochemical transformations between different ocean regions by providing a link between cellular and community level processes.



DECLARATION OF THE CONTRIBUTION TO EACH CHAPTER

Chapter 2

This chapter has been published in *Frontiers in Marine Science*. The publication is titled “Thermal performance curves of functional traits aid understanding of thermally induced changes in diatom-mediated biogeochemical fluxes”, and the authors are; Kirralee G. Baker, Charlotte, M. Robinson, Dale T. Radford, Allison S. McInnes, Christian Evenhuis, and Martina A. Doblin. I was responsible for conception of the experiment, methodological development, data interpretation and write-up of the manuscript. I was responsible for 2-(4-pyridyl)-5-((4-(2-dimethylaminoethylaminocarbamoyl)methoxy)phenyl)oxazole (PDMPO) assays, growth and cell size data. Dr. Allison McInnes (UTS) and myself conducted flow cytometry analyses. Assoc. Prof. Martina Doblin (UTS) conducted the primary productivity assays and Charlotte Robinson (UTS) collected photophysiology data. I was mostly responsible for post-processing of samples, with assistance in nutrient analysis from Dale Radford (UTS). I was mainly responsible for data analysis, with assistance in bootstrapping of data from Dr. Christian Evenhuis (UTS).

Chapter 3

The data presented in this chapter was a joint laboratory effort. I was responsible for conception of the experiment, methodological development, data analysis and interpretation, and write-up of the manuscript. Biogenic silicon production and PDMPO assays were conducted by myself. Source water collection and characterisation (primary productivity and pigment analyses) were conducted by Marco Alvarez-Rodrigues (UTS). Dr. Allison McInnes (UTS) and myself conducted flow cytometry analyses. Assoc. Prof. Martina Doblin (UTS) conducted the primary productivity assays and Charlotte Robinson (UTS) collected photophysiology data.

Chapter 4

The majority of the data presented in this chapter was collected by myself during the SS2013-t03 voyage in northern Australia (RV Southern Surveyor, July-August 2013). Assoc. Prof. Martina Doblin (UTS), Assoc. Prof. Justin Seymour (UTS), Lauren Messer (UTS) and Charlotte Robinson (UTS) were key contributors securing ship time for this voyage. I was responsible for conception of the experimental design, methodology development, data analysis and interpretation, and write-up of the manuscript. Biogenic silicon production, PDMPO and nitrate addition assays were conducted by myself. I also collected the particulate organic matter and phytoplankton pigment samples, these samples were processed by Lauren Messer (UTS) and Charlotte Robinson (UTS). Dr. Daniel Nielson (UTS) and Dale Radford assisted with image analysis and Dr. Penelope Ajani assisted with phytoplankton identification.

Chapter 5

The data presented in this chapter was a joint laboratory effort. I was responsible for conception of the experimental design, methodological development, data interpretation, and write-up of the manuscript. I was responsible for the collection of the growth, cell size, photophysiological data. Dale Radford (UTS) assisted with nutrient analyses and I assisted Dr. Unnikrishnan Kuzhiumparambil (UTS) with fatty-acid methyl esters (FAME) analysis. I was mostly responsible for data analysis, with assistance in bootstrapping of data from Dr. Christian Evenhuis (UTS). Assoc. Prof. Martina Doblin (UTS) conducted the primary productivity assays and Lisa Hou (UTS) initially established the laboratory cultures used for this experiment.